Simple Book Example

TeXstudio Team

January 2013

thesis

Contents

List of Figures

Chapter 1

Simulations of a plenoptic 1.0 system

1.1 Introduction

In this chapter results are presented form simulations of plenoptic 1.0 raw data using the simulation platform described in chapter **??**. The methods used to design, develop and test the data processing algorithms, such as rendering, synthetic refocus and depth estimation algorithms, from the digitally generated light fields data are described. All the light field processing algorithms presented in this chapter use the third parametrization of the light field, described in **??**, that is the four dimensional representation of the intensity recorded on the sensor. Each point of this four dimensional array is a ray at the position x and y with a direction θ_x and θ_y [2, 3].

1.2 Description of the system

The plenoptic 1.0 camera described in section **??** has been modelled as a 2f system composed by a main lens, a micro lens array and a sensor as shown in figure 1.1. The micro lens array is placed at a distance $z=2f$ form the main

lens, where f is the focal length of the main lens, and the sensor is placed at a distance f_μ from the micro array plane that is also the focal length of the lens lets. In this configuration the lens let array plane is conjugated with the object plane, while the sensor plane is conjugated with the main lens plane. In order to satisfy the f-number matching condition described in section **??** once the propagation distances, the micro lens array parameters, the resolution N of the input field, the wavelength of the light used and the micro array parameters, the software automatically sets the aperture of the main lens.

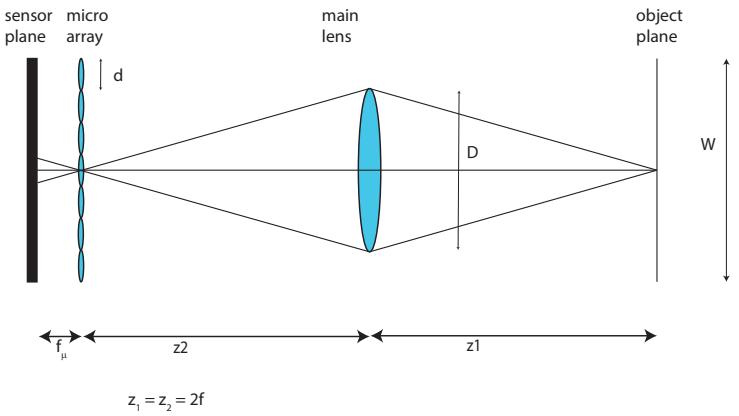

Figure 1.1: The parameters that characterize the micro lens array are: the pitch p, defined as the distance between the centres of two lens lets, the diameter d, the number of lens lets per raw N and the size of the micro array W.

The micro array parameters are illustrated in figure 1.2 and are the pitch, the diameter of the single lens let, the number of lens let in a row and the size of the array. In all simulations the pitch of the lens lets is taken equal to the size of its diameter and the lens lets are arranged in a square matrix.

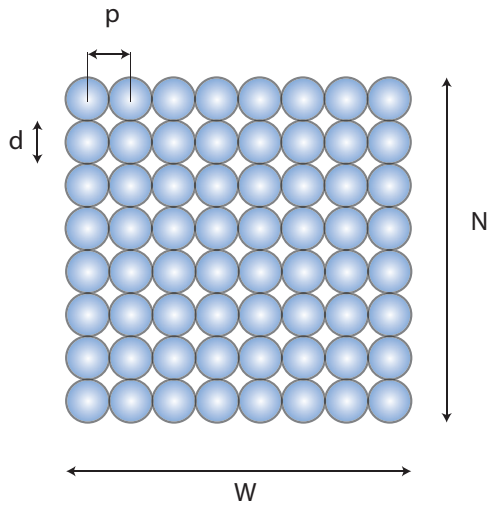

Figure 1.2: The parameters that characterize the micro lens array are: the pitch p, defined as the distance between the centres of two neighbouring lens lets, the diameter$d$, the number of lens lets per row N and the size of the micro array W.

1.2.1 Diffraction effects on the System

During the development of this work has been noted that diffraction from the lens let circular aperture generates cross talk between neighbouring sub images since the light form a single lens let falls in the sub image of the neighbour lens let. Because of this, blur is present in the rendered image resulting in a loss of spatial resolution. To avoid this loss of resolution the diameter of each lens let should be large enough so that the diameter of the Airy disk is totally smaller than the lens-let diameter. As seen in equation **??** for a lens with a circular aperture, the diameter of the Airy disk at its focal plane is

$$d_{Airy} = 2.44\lambda z/D \tag{1.1}$$

In order to avoid diffraction induced cross talk the lens let diameter should be at least the same diameter as the Airy disk so that the diffraction pattern is included in the sub image until its second zero:

$$D > 2.44\frac{\lambda z}{D} \tag{1.2}$$

Therefore the condition of D is:

$$D > \sqrt{2.44\lambda f_{\mu}} \tag{1.3}$$

Therefore when choosing a or designing a lens let array for plenoptic imaging, the lens let diameter and the focal length should satisfy equation 1.3. The acceptable values belongs to the area above the blue line in the diagram shown in figure 1.3.

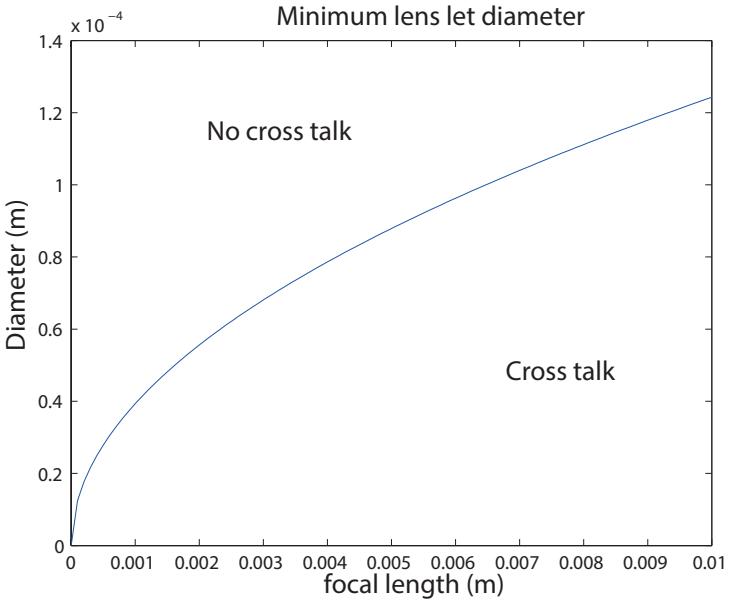

Figure 1.3: Values of acceptable lens let diameter to avoid diffraction induced cross talk.

The effect of cross talk between lens lets on the raw image is shown in figure 1.4.

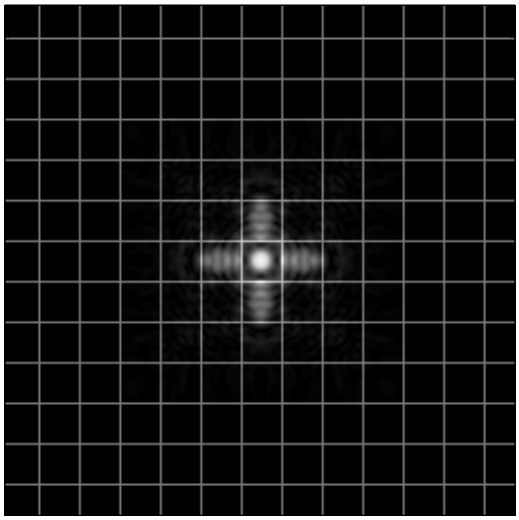

Figure 1.4: Raw image of a point source.The grid represents the edges of the sub images. If the point source is in focus, it should be represented by only one lens let. Because of diffraction some light goes also on the neighbouring sub images.

Figure 1.5 shows what happen in the phase space of point source in presence of cross talk and without cross talk. In the first case there is no blur since all the light coming from a point source in focus is recorded by a single lens let, while in the second case the spreading of the light due to diffraction causes a blur that is proportional to the number of sub images involved.

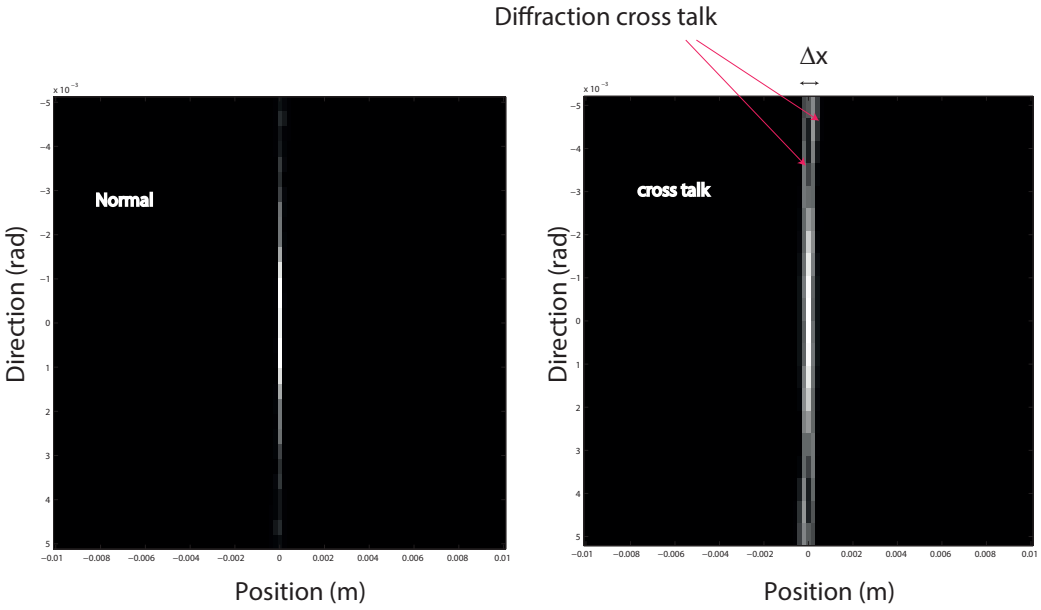

Figure 1.5: Phase space of the light field of a point object: on the left when the condition 1.3 is respected; on the right when diffraction induces cross talk arise between neighbours lens lets. Cross talk introduces a blur in the rendered image whose width is Δx.

1.3 Advanced Rendering Techniques

As described in chapter **??**, one pixel in the rendered image is obtained as a mean of all the pixels of the sub image that corresponds to the position of the pixel in the final image [2]. This method generates an image that is equivalent to the image obtained with a conventional camera without any additional information. Since the final resolution depends on the number of lens lets in the micro array, it will be smaller than the resolution that can be obtained by a conventional camera which instead uses the full sensor resolution [3]. To use the full variety of features enabled by light field imaging, more advanced post processing techniques of the raw data should be used. The first two post processing features presented are the change of aperture

and of point of view. These effects are achieved by integrating each sub image along a sub set of directional coordinates, hence on a smaller number of pixels.

1.3.1 Changing Aperture

The quality of the image captured by a conventional camera depends on the combination of shutter speed and aperture chosen in order to get the optimum total exposure [52]. The possibility to change the aperture of the main lens in post processing allows to change the depth of field of the final image. In the simulations presented in this work the shutter speed is not an issue since all the objects imaged where static with constant and uniform illumination. Therefore what determines the exposure is the aperture of the main lens or the f-number. The f-number is proportional to the depth of field of the imaging system that can be defined as the range of depths that appears sharp in the resulting photograph [2]. If the f-number increases and the aperture gets smaller, the depth of field increases. Therefore a plenoptic camera can control the depth of field in post processing. Looking at the raw plenoptic image, each sub image is formed by a number of samples of the directions of the rays. If in equation **??** the range of integration along the directional coordinates is reduced, the aperture of the main lens is reduced af the same amount. If the aperture is smaller the rays propagating with an high angle respect the optical axis will not reach the sensor and will be not considered to form the intensity of each pixel. The result is a rendered image that looks like it has been captured with a narrower aperture. Computationally the

algorithm to reduce the aperture is:

$$I(x,y) = \frac{1}{N'^2} \sum_{i=k/2}^{N-\frac{k}{2}} \sum_{j=k/2}^{N-\frac{k}{2}} L(x,y,i,j) \tag{1.4}$$

where $N' = N - k$ and k is the range of directional coordinates considered in the sum. This operation in the phase space is shown in figure **??**:

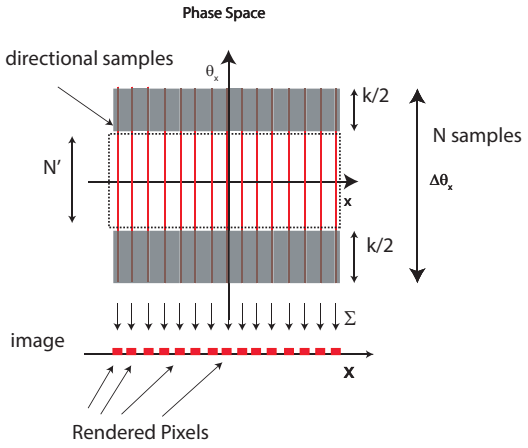

Figure 1.6: Rendering seen from the (x, θ_x) slice of the phase space. The directional pixels not considered for the integration are shown in grey.

An effect of reducing the aperture of a camera is to extend its depth of field. Therefore the depth of field can be digitally extended changing the range of directional coordinates included in the sum as explained above. In figure 1.7 is shown the raw image of thin silky skin separating two layers of an onion, immersed in oil to improve transparency obtained by Levoy *et al.* in Stanford University [4].

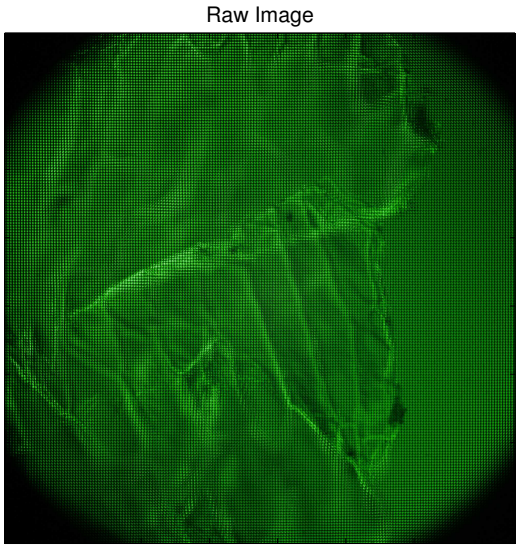

Figure 1.7: Raw plenoptic 1.0 image obatined from Levoy *et al.* The microscope was a Zeiss Axiovert with a 20x/0.5NA (dry) objective. The micro lens array was 24mm x 36mm, with square 125-micron x 125-micron f/20 micro lenses, held in front of the Axiovert's side camera port using an optical bench mount. The camera was a Canon 5D full-frame digital SLR. The specimen was the thin silky skin separating two layers of an onion, immersed in oil to improve transparency [4].

Figure shows 1.8 the differences between the rendered image integrating over the full aperture, and the rendered image obtained using only the central pixel of each sub image. The effect is to reduce the aperture to a pinhole and to have an all-in-focus image. Images has been obtained with home made rendering algorithm written in MATLAB. parating two layers of an onion, immersed in oil to improve transparency.

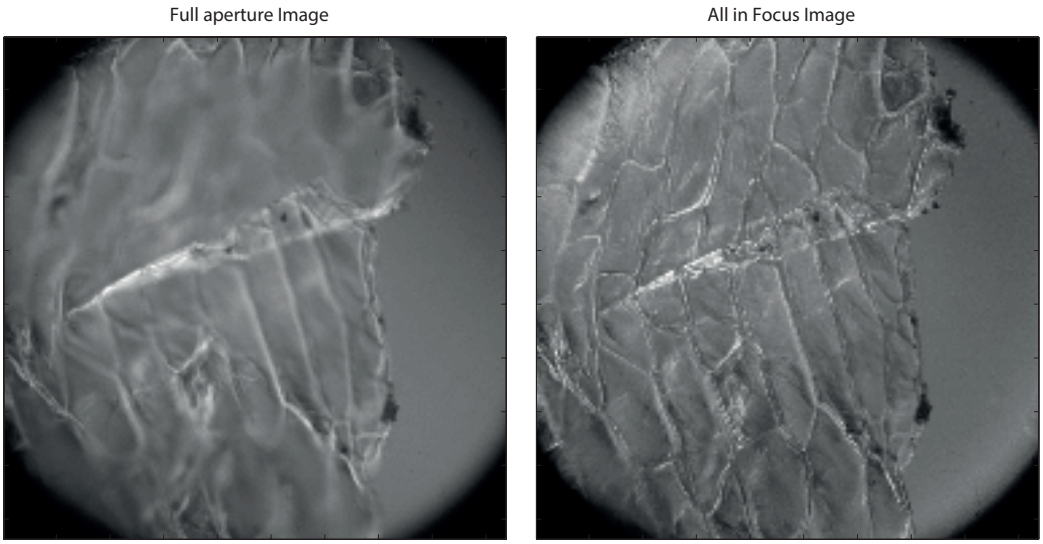

Figure 1.8: Rendered Images from the raw data in figure 1.7. On the left there is the full aperture imagea, obtained integrating along all the directional coordinates while on the right there is the all in focus image obtained taking onli the central pixel of the each sub image, that corresponds to rays with the direction parallel to the optical axis.

1.3.2 Changing the point of view

It is possible to change the point of view in the rendered image integrating along a all the directional coordinates in one direction keeping fixed the other direction. For example an image corresponding to a particular point of view can be obtained, with reference to equations 1.5, keeping fixed the

$$\begin{aligned} I(x,y) &= \frac{1}{N}\sum_{i=0}^{N} L(x,y,i,k_y) \\ I(x,y) &= \frac{1}{N}\sum_{j=0}^{N} L(x,y,k_x,j) \end{aligned} \tag{1.5}$$

1.4 Depth estimation

In this section it will be explained how it is possible to extract depth information from light fields data. In the specific case of plenoptic 1.0 raw data,

depth can be decoded looking at the phase space. In section **??** is explained that a point source on the focal plane of the main lens looks like a straight vertical line in the phase space. The physical meaning of this is that for a single position, one lens let, all the directional coordinates are sampled[3]. If the point source is out of focus the situation is different. If the source is closer to the main lens with respect to the focal plane, it will be imaged on a plane that is behind the micro array. This situation is shown in figure 1.9. Both directional and positional coordinates are sampled by more than one lens let and each sub image will sample a set of directional coordinates correspondent to the part of the main lens from where the rays come from. Figure 1.10 shows what happens in the phase space. On the lens let plane the spot size will have a width of Δx proportional to the distance, therefore the directions will be sampled by the lens lets included in this interval. Each lens let receives light coming form a particular area of the main lens, its correspondent sub image only records the pixels linked with those coordinates as can be seen comparing figure 1.9 with 1.10. The resultant phase space representation is still a straight line, but with positive slope proportional to the distance of the point source 1.10. If the source is further away from the plane where the main lens is focused, the main lens image is formed before the lens lets plane. The point is still sampled by more than one lens let included in the spot size Δx. The difference with the previous case is that now in the phase space the point source is represented by a straight line with a negative slope. The physical meaning of the slope of the phase space line can be understood by looking at figure 1.11. When the main lens image is formed in front of the micro lens plane the increasing directions on θ_x axis are

mapped on decreasing positions on the x axis and the line on the phase space representing the point has a negative slope. If the image is formed behind the micro lens plane increasing directions on θ_x axis are mapped on increasing positions on the x axis this inversion is absent and the line in the phase space has a positive slope [2]. This characteristic of the phase space permits to discriminate between points in the scene that are in front or behind the main lens focal plane, giving a first rough depth estimation.

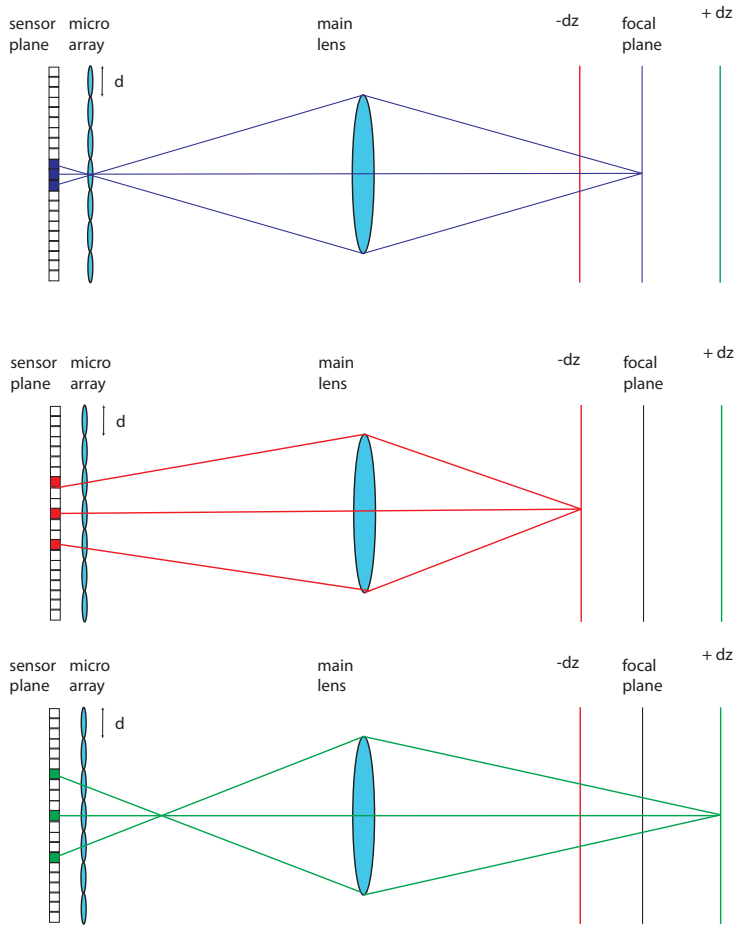

Figure 1.9: Sampling of the light field of a point source in focus, on the top, closer to the main lens, centre, and further away, bottom. When the source is out of focus, both position and directions are sampled by more than one lens let since the main lens image is not formed any more on the lens let plane.

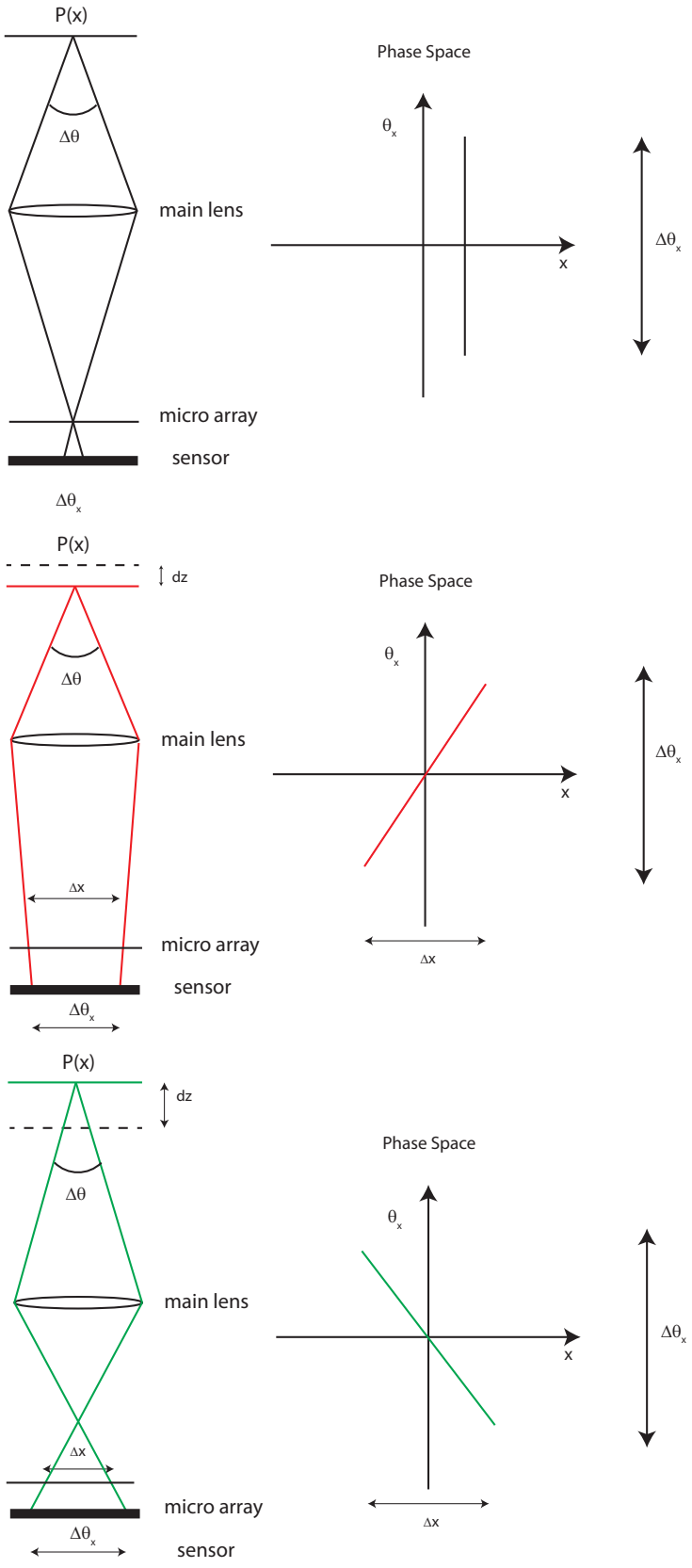

Figure 1.10: Information on the depth of a point source imaged by a plenoptic 1.0 system. As explained in section **??** If the point source is in focus, on the top, it's position is sampled by one lens let as well as the whole set of directions .

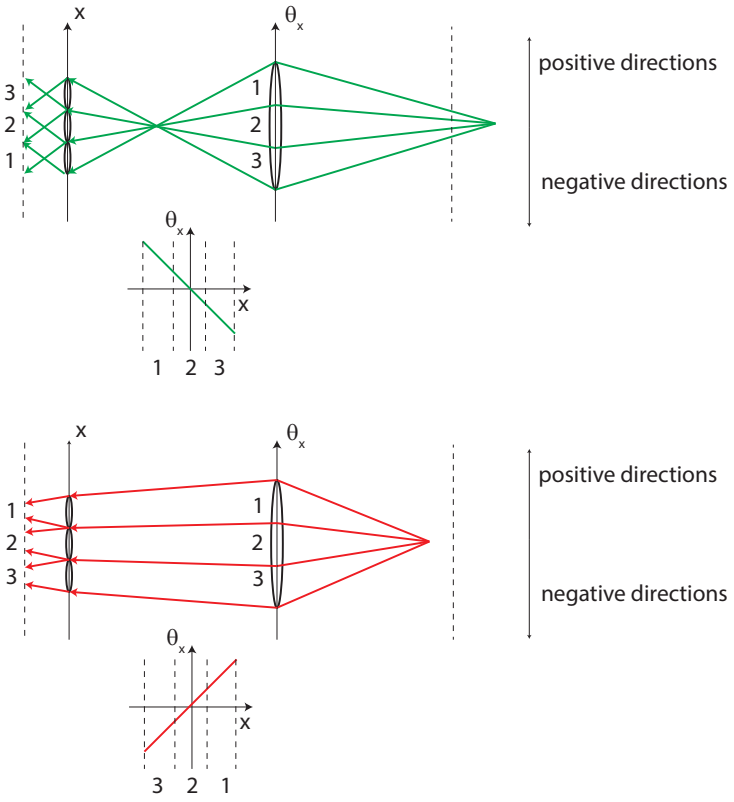

Figure 1.11: Physical meaning of the slope in the phase space. If the point source is further then the camera focal plane, the phase space line has a negative slope. If the point source is closer then the focal plane, the slope of the phase space line is positive.

A simulation of plenoptic 1.0 camera has been made to verify this fact. The system was composed by a main lens with a focal length of *120 mm*, in a *2f* configuration creating an image on the micro array plane. The Micro lens array was composed by a matrix of 101 by 101 lens lets with a diameter of 100 μm and a focal length of 100

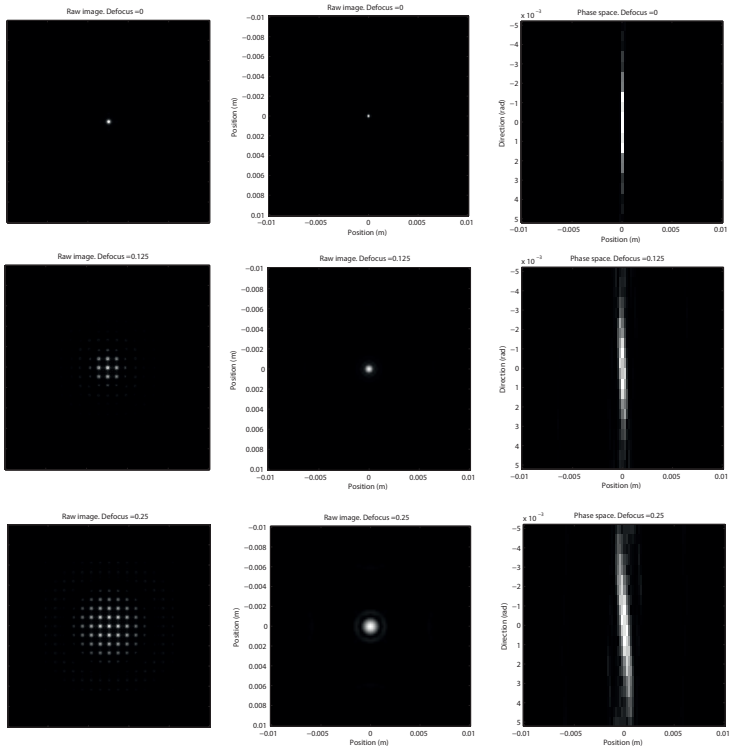

Figure 1.12: Numerical simulation of a point source imaged by a plenoptic 1.0 imaging system. The point source was placed at three different distances from the main lens. The top three figurers show the focused image. in the centre ones a defocus of 0.125 m is added and the point source is further away from the main lens. In the bottom ones the point source is closer to the main lens of .25 m. In all the three cases the raw data image is on the left, the rendered image is on the centre and the phase space line is on the right.

1.5 Synthetic refocus

Another post processing feature enabled by collecting the light field is the possibility to refocus an image after it has been captured. This features is called synthetic refocusing and is based on the fact that the recorded light field can be used to compute images as if they were taken by a synthetic camera positioned and focused differently form the actual camera. In this

section the synthetic refocus algorithm is explained according to what is treated in the research work of Ng *et al.* [21, 2]. This method is based on the fact that it possible to define a synthetic camera composed by an aperture and a sensor plane, for which the defocused object plane results in focus. It will also be explained how this method, based on a synthetic camera model obtained with ray tracing, can be implemented in a wave optics approach using the simulation platform developed in this work and the limitations and the issues arising from a wave approach respect the simple and ideal ray optics approach will be discussed. Figure shows 1.13 a plenoptic 1.0 imaging system whose main lens produces an out of focus image on the micro lens plane. The directional set of coordinates Δu is mapped along the range of spatial coordinates Δx. The light field can be re parametrized in terms of a synthetic light field generated by an aperture on the plane *u'* represented by the dashed lens, that focuses the object on a synthetic focal plane, *x'*. This second light field is parametrized with the coordinates *u' v'* and *x' y'*.

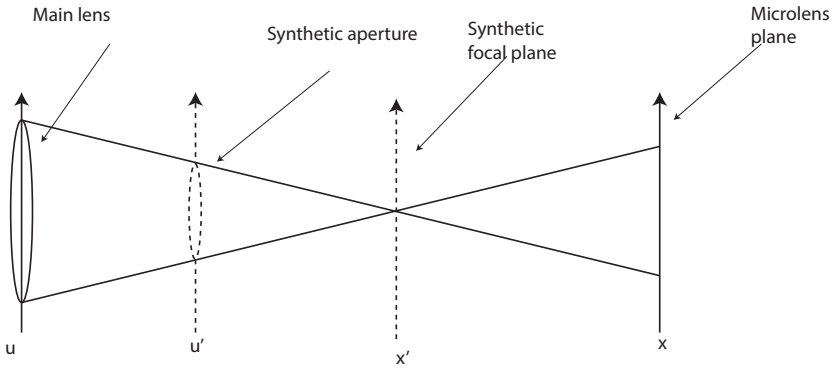

Figure 1.13: The synthetic camera refocusing method is based on the fact that is always possible to define a virtual aperture that is focused on the lens let plane.

As explained by Ng [21] and in analogy with what was explained in section

?? it is possible to define the intensity obtained rendering a synthetic light field $L'(x', y', u', v')$ at the synthetic focal plane as:

$$I(x, y) = \iint L'(x', y', u', v')A(u', v')dudv \tag{1.6}$$

The goal is to express this intensity as a function of the captured light field $L(x, y, u, v)$ presente on the actual sensor plane, finding the relationship that links the set of coordinates *x,y,u,v* with *x',y',u',v'*.

1.5.1 Synthetic refocus algorithm

To find the link between the real and the synthetic light field do the following simplifications are made:

- only the synthetic sensor plane *x',y'* will be moved. Therefore the main lens plane *u',v'* is at the same position of the plane *u,v*, and no transformation is performed on the directional coordinates, therefore *(u,v)=(u',v')*.

- the aperture of the main lens will not change, $A(x', y') = 1$.

Figure 1.14 shows a two dimensional diagram explaining the re-parametrization under the hypotheses explained above. Only shows the coordinates x and u are shown for simplicity. F is defined as the distance of the main lens from the lens let array plane, and F' as the distance from the synthetic focal plane. The ratio between these two distances is the refocusing parameter α, defined as:

$$\alpha = \frac{F}{F'} \tag{1.7}$$

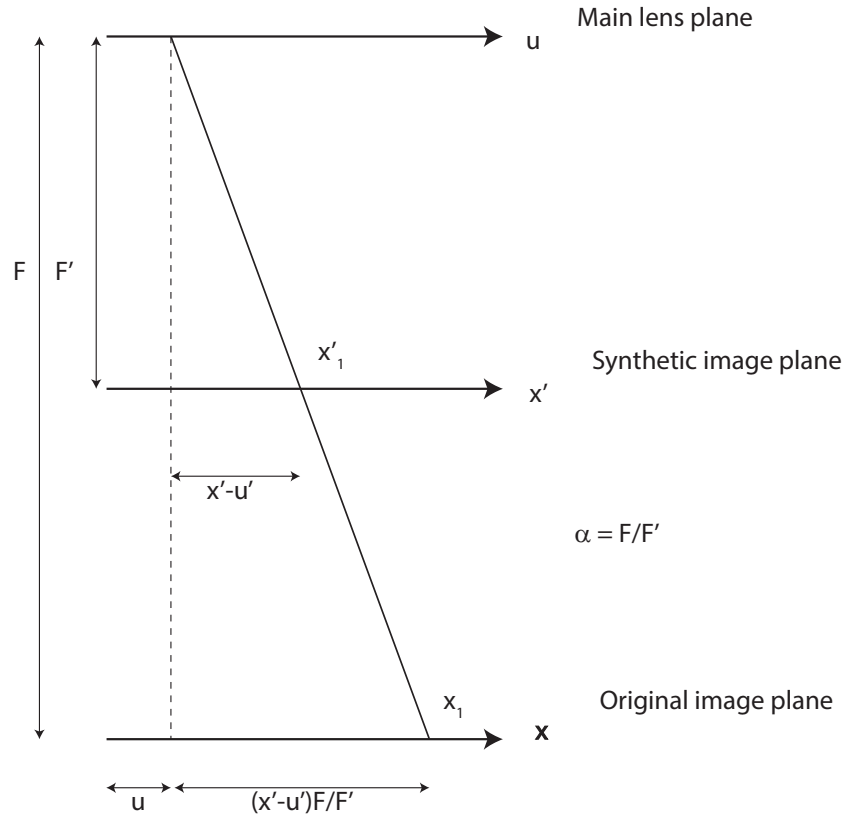

Figure 1.14: Changing the focal plane of the camera is equal to re parametrize the light field according to the new coordinates. The re parametrization is basically a shift proportional to the ratio between the refocused plane and the original camera plane α .

The refocusing factor can assume the following values:

- $\alpha = 1$ when the synthetic focal plane is at the same position of the main lens focal plane

- $\alpha > 1$ when the distance between the main lens and the synthetic image plane is smaller than the distance between the main lens and its original focal plane. This occur when the system is refocused on a plane that it is further away with respect to the main lens focal plane.

- $\alpha < 1$ when the distance between the main lens and the synthetic image plane is bigger than the distance between the main lens and its original focal plane. This occur when the refocus take place on a plane that it closer with respect to the main lens.

Looking at figure 1.14 a ray of light that crosses the main lens plane at the coordinate u and that then intercepts the synthetic image plane at the point x_1', can be represented using with the coordinates of the original image plane x_1. Because of similar triangles, the value of the x coordinate on the image plane can be expressed as a function of the coordinates u, x'. We have:

$$x_1 = u + (x_1' - u)\frac{F}{F'} = u + (x_1' - u)\alpha \tag{1.8}$$

Therefore extending to the four dimensional case, the points belonging to the synthetic image plane can be expressed as a function of the directional coordinates at the main lens plane and the spatial coordinates at the original image plane as:

$$\begin{aligned} x' &= \frac{x}{\alpha} + u\left(1 - \frac{1}{\alpha}\right) \\ y' &= \frac{y}{\alpha} + v\left(1 - \frac{1}{\alpha}\right) \end{aligned} \tag{1.9}$$

With this change of coordinates the light field at the synthetic focal plane x' can be written substituting equations 1.9 into equation 1.6.

$$I(x,y) = \iint L\left(\frac{x}{\alpha} + u\left(1 - \frac{1}{\alpha}\right), \frac{y}{\alpha} + v\left(1 - \frac{1}{\alpha}\right), u, v\right) A(x', y')dudv \tag{1.10}$$

Equation 1.10 represent the rendered image obtained integrating along the directional coordinates the light field re parametrized as if it were captured by a camera whose focal plane is the same as the synthetic focal plane.

Focusing at different depths corresponds to changing the separation between the lens and the film plane, shifting it of a quantity proportional to the refocusing factor α. From equation 1.9 the four dimensional the light field at the synthetic plane is obtained from the light field recorded on the sensor by shifting and rescaling its spatial coordinates. The transformation operated on the light field is the composition of two transformations:

- a scaling of a factor α that depends by the distance of the synthetic focal plane from the main lens.
- a translation term $u(1 - 1/\alpha)$ that increases with the directional coordinates and with the magnitude of the factor alpha.

Therefore the synthetic refocus can be treated as a linear operator acting on the four dimensional light field that maps the light field recorded on a new set of coordinates. The rendering on this new set of coordinates gives the image focused at a different plane.

1.5.2 Refocusing Operator

The synthetic refocus equation 1.10 has been obtained with ray optics considerations only. However, it can be applied to light fields obtained light fields obtained with wave optics simulations. This novel approach to implement the refocusing algorithm to a synthetic generated wave optics is one of the main result of this work. When using wave optics particular attention should be given in the design of the imaging system in order to avoid cross talk effects induced by diffraction, as explained in section 1.2.1. The effects of this operator in the phase space is a change of the slope of the lines

describing the points of the image in the phase space. Since the total light field is conserved, the area in the phase space remains the same, hence the projection of the light field on the phase space results sheared respect the original one.

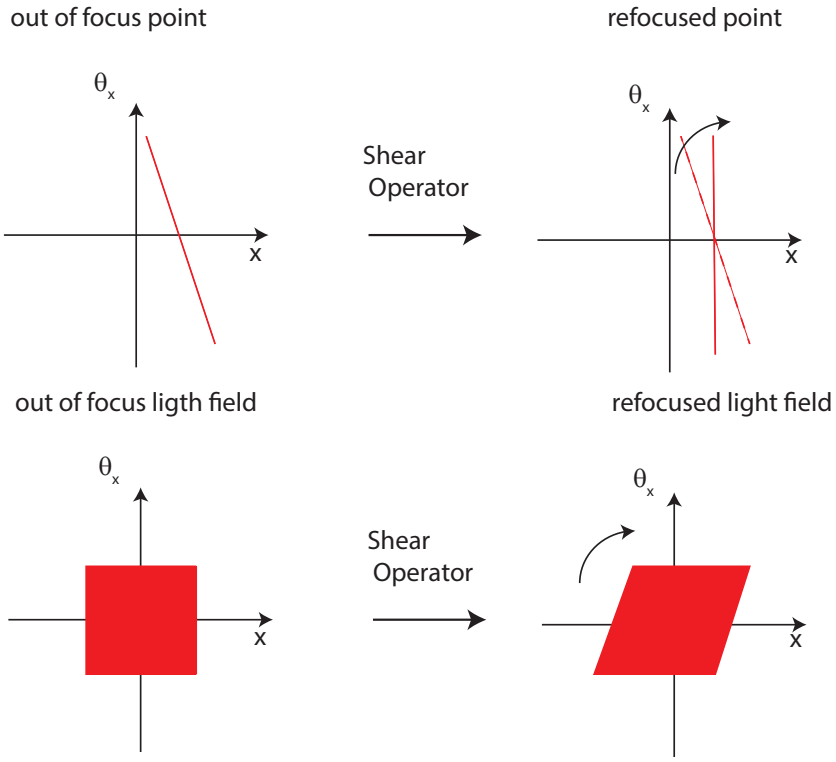

Figure 1.15: Changing the position of the focal plane is equal to shear the light field in the phase space. The total area remains the same since the total light field is conserved.

A MATLAB piece of code has been developed to implement the synthetic refocus operator. The algorithm is composed by two distinct stages. The first stage creates a new set of spatial coordinates shifting and rescaling the the original set of coordinates as shown in equation 1.9. Then the output synthetic light field is created interpolating the input light field using as a base the new set of coordinates. The flow chart can be seen in figure 1.16

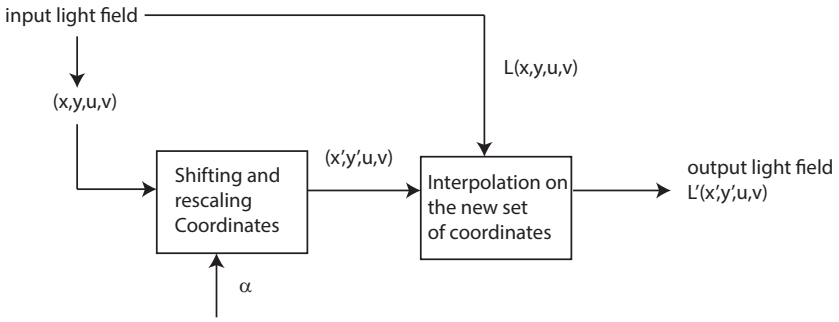

Figure 1.16: Flow chart of the operator shearing.

1.6 Results of the Simulations

To test and explore the potentials of the synthetic refocusing algorithm has been used wave optics simulation toolbox described in section **??**. The System simulated is the one described in section **??** and shown in figure 1.17. The optical parameters can be found in the following table.

Main lens focal length f	120mm
Lens aperture D	3.6 mm
Micro lens focal length f_μ	10 mm
Micro lens diameter d	150 μm
Micro array pitch p	150 μm
Field of view W	20 mm
f-number	33.6
sensor resolution	3030 by 3030 pixel

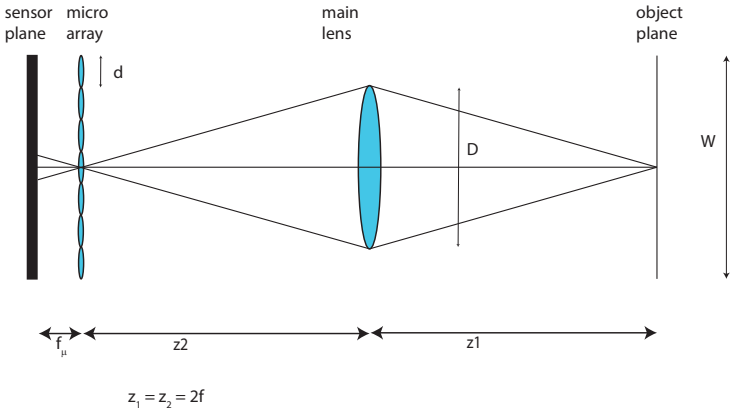

Figure 1.17: Set up simulated.

With this set up the final rendered image resolution is of 101 by 101 pixel. Each pixel of the final image corresponds to a lens let, therefore the spatial resolution the final image is equal to the diameter of the single lens let. Each sub image has 30 by 30 pixels, meaning that the full set of directional coordinates is sampled by $N_{sub} = 30$ samples. The angular resolution is therefore:

$$\delta\theta = \frac{\Delta\theta}{N_{sub}} = \frac{NA}{N_{sub}} \tag{1.11}$$

and is equal to $\delta\theta = 2.510^{-4} rad$.

The first object to be imaged was a volume V of dimension 20 mm x 20 mm x 100 mm containing three point sources. Each point source has been simulated by a circle of 10 μm diameter and are positioned as shown in figure 1.18

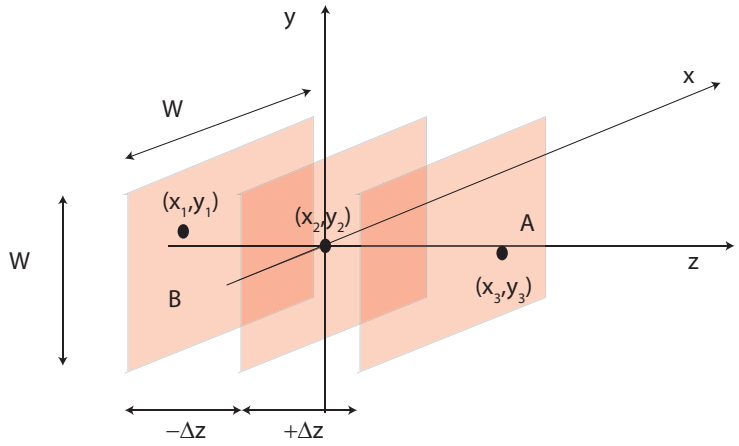

Figure 1.18: Position of the point sources imaged inside the volume V simulated.

Each plane has been imaged singularly setting the distance z_1 equal to the sum of the distance of the main lens focal plane and the defocus δz. The Coordinates of the points are:

- A: $x_1 = -3, y_1 = -3, z_1 = -50$
- B: $x_2 = 0, y_2 = 0, z_2 = 0$
- C: $x_3 = +3, y_3 = +3, z_3 = +50$

After that the light of the three planes has been propagated into the system, the final raw image has been obtained summing the three separate raw images normalized by the total amount of energy contained. This can be done since the Fresnel simulation toolbox is time independent. Figure 1.19 shows the total raw image and the rendered image integrated without any refocusing. 1.18

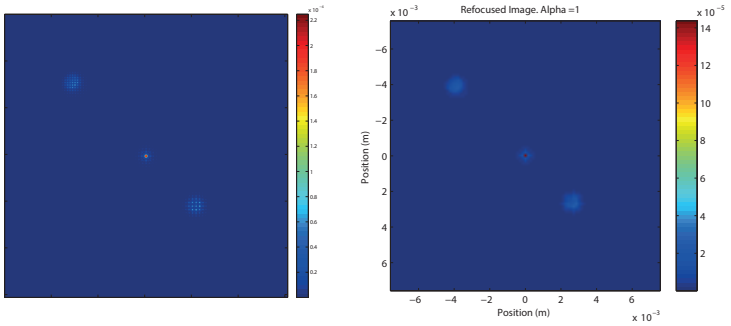

Figure 1.19: Raw image on the left and rendered image on the right. Intensity is shown in false colour in order to appreciate variations in energy distribution.

The central spot is in focus, since the point source is at a distance of $z = 2f$ on the main lens focal plane. For a defocus of 50 mm the factor α can be obtained from the lens equation. For the 2f system simulated and referring to figure 1.14 for notations:

$$\frac{1}{f} = \frac{1}{F'} + \frac{1}{z + \Delta z)} \tag{1.12}$$

Since $\alpha = F/F'$, and in a 2f system F=2f=z:

$$\frac{1}{f} = \frac{\alpha}{2f} + \frac{1}{2f + \Delta z)} \tag{1.13}$$

Resolving for α becomes:

$$\alpha = \frac{2f + s\Delta z}{2f + \Delta z} \tag{1.14}$$

Figure shows the values of α obtained by equation1.14 for defocus varying between plus and minus 10 cm.

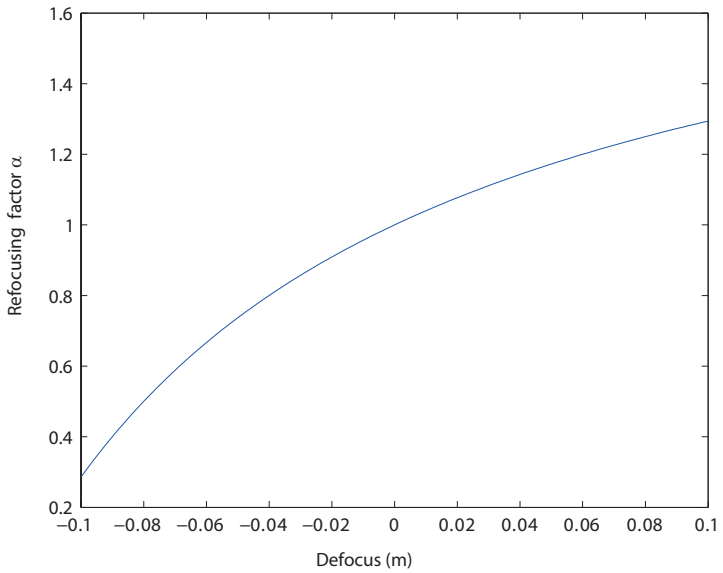

Figure 1.20: Values of the refocusing factor α as a function of the defocus. A positive defocus means that the object it further away with respect to the main lens, a negative defocus indicates an object that is closer.

We can see from figure 1.20 that, as expected, the refocus factor is not linear with defocus and therefore the axial resolution in not linear. When the object is closer to the the main lens, small variations in the defocus give large variations in α while the opposite happen when the object is further away with respect to the main lens.

Figure 1.21 shows the refocused imaged obtained from shearing the light field extracted by the raw image in . According to equation 1.14, the point A is refocused for a value of α equal to 0.7 and point B for $\alpha = 1.17$.

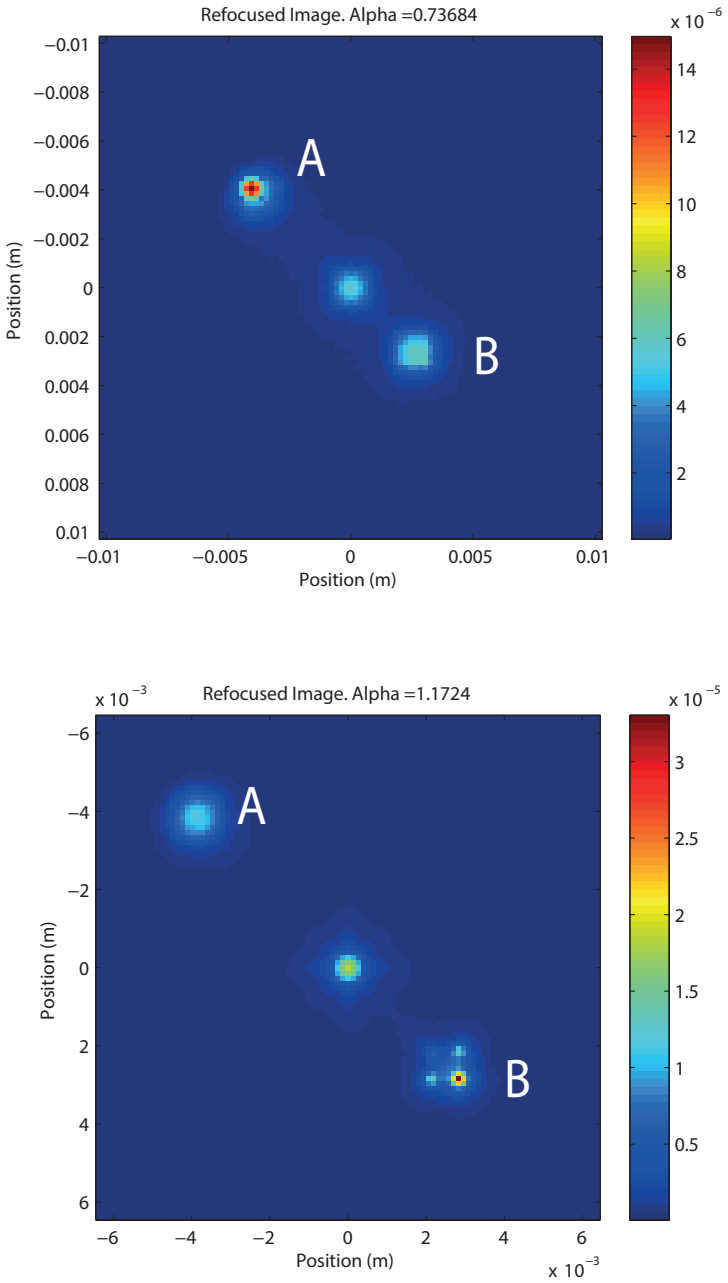

Figure 1.21: Refocused Images of the three point sources in image 1.19. In the top one the point A is refocused, in the bottom one the point B is refocused. The colour bar indicates the how the intensity is distributed. When the point source is refocused, the intensity distribution is higher with respect to the out of focus points.

The effects of the refocusing operator can be appreciated looking the intensity values of the refocused point sources. In the top image of figure 1.21 the point labelled with the letter A is refocused, and the majority of the light present in the photo concentrates on its location. The same happens in bottom figure, where the brightest point, indicated in red according to the colour bar, is the refocused one (B). This is a proof of the fact that the refocusing operator, shearing the four dimensional light field, simply move the intensity from a location to another. The Total energy of the image remains unchanged.

1.7 Focal stack depth estimation

The synthetic refocus algorithm provides a method to estimate the depth of a point source in a volume. Looking at the Fourier transform of a rendered image of a point source before and after the refocusing operation can be seen that when the point source is in focus, its spectrum is broader than the blurred one. This fact is true for normal images as well, when the presence of sharp details in the focused image, causes its spectrum to have a larger amount of high spatial frequencies, and therefore a bigger energy distributed on the nigh frequencies. In figure is shown the difference between the spectrum of the out of focus image(blue) and the in focus image(red) for a defocus of 5 cm.

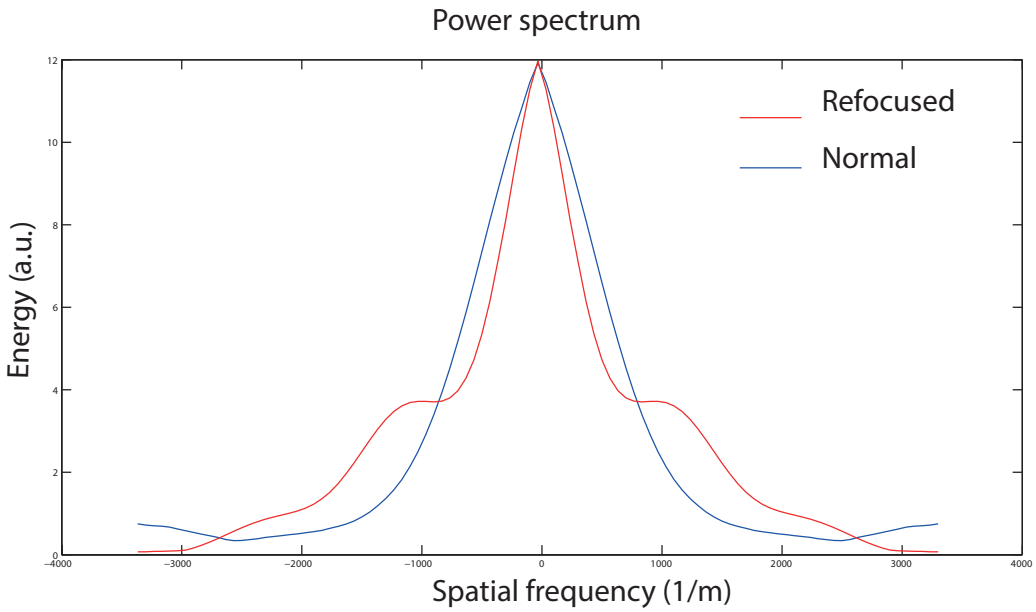

Figure 1.22: Refocused images...

The action of shearing the light field produces a redistribution of the power spectrum of the signal towards high frequency. This effect causes the sharpness of the image and therefore the refocus. This effect can be used to estimate the depth of object imaged just evaluating its level of blur. This blur based depth estimation is an original contribution of this work to light field literature. The method consists in creating a focal stack shearing the light field at different values of the coefficient alpha, that correspond to different focal planes, and rendering the images. After the focal stack is created the power spectrum of each image is calculated using the fast Fourier transform algorithm. The low frequency terms are then removed high pass filtering the images and the total energy contained in the high frequency term is calculated integrating the Fourier spectra. Plotting the values of energy as a function of the different alpha coefficients a curve with a maximum in the

proximity of the most in focus image is obtained. This maximum corresponds to the image in the focal stack that best estimates the actual value of alpha. In figure 1.23 are shown the energy as a function of the refocus parameter alpha for a point source placed at different depths. The vertical red line indicate the position of the maximum. The values of the estimated alpha and the real one are shown in the following table:

Estimated α	Real *alpha*	Error	Defocus
0.85	0.738	0.1132	-0.05 m
0.925	0.8837	0.0413	-0.025 m
1.080	1.0943	-0.0143	+0.025 m
1.105	1.1724	0.0674	+0.05 m

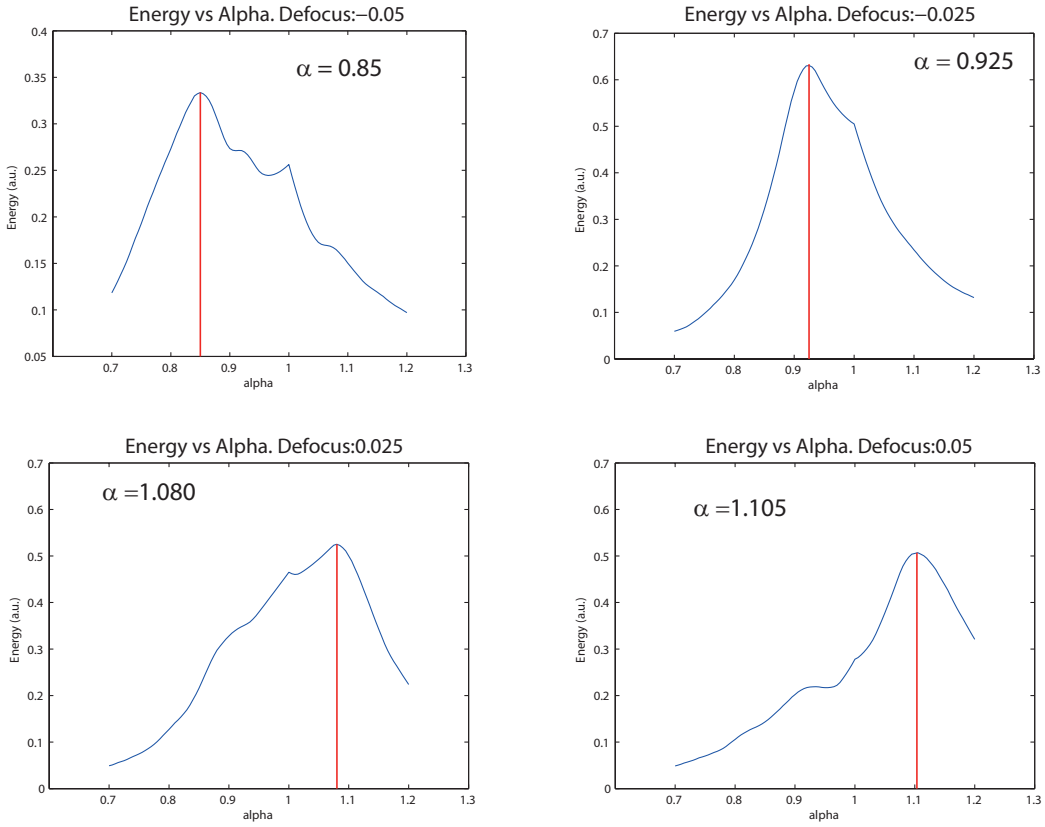

Figure 1.23: Refocused images...

Figure 1.24 shows the distribution of the estimated values of alpha versus the actual values obtained from equation 1.14. The estimated values for a defocus of -0.1 m and - 0.08 m are equal to 1 as if the image would lie on the focal plane. These are clearly wrong estimation and represent a limitation for the method described. It is interesting to see that for negative defocus the parameter α is over estimated and the error is positive while for positive defocus the error is negative. The minimum error is present for values of defocus corresponding to positions close to the focal plane. The error in the estimation of the refocusing factor is plotted in figure 1.25.Having seen these results the method has a better accuracy in a range of depth around the focal

plane and looses when the absolute value of the defocus increase.

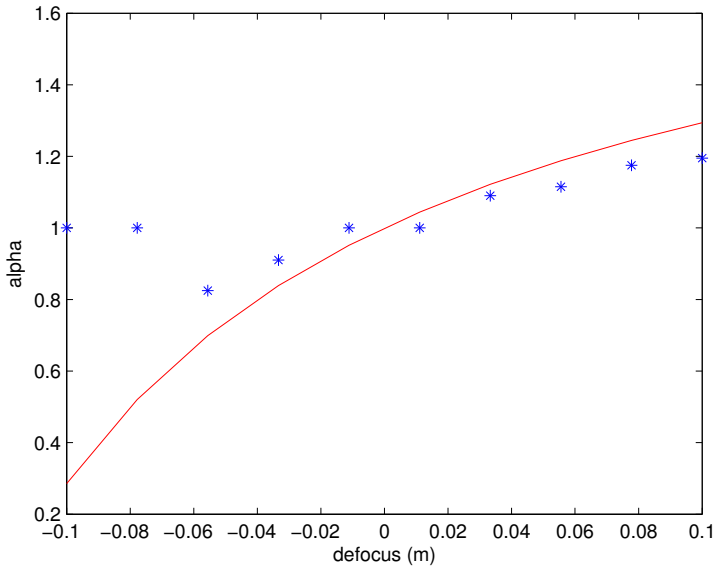

Figure 1.24: Estimated values of α represented by blea stars and the theoretical values represented with the blue line.

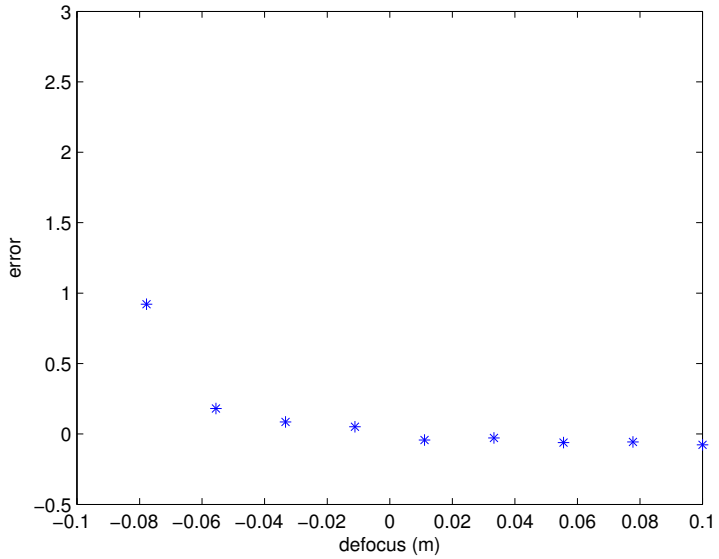

Figure 1.25: Distance between the estimated values of alpha and thje actual theoretical values.

These results show that the depth evaluation depends from the distance

of the object from the camera. This is a natural consequence of the non linearity of tghe lens equation. A way to have a linear dependency of the parameter alpha with the refocusing distance is to have an array on lenslet with variable focal length [6, 27], or changhing the focal length of the lens lets dynamically using electro optics effects [57].

Bibliography

[1] Shree K Nayar. Computational cameras: Redefining the image. *Computer*, (8):30–38, 2006.

[2] Ren Ng. *Digital light field photography*. PhD thesis, stanford university, 2006.

[3] Todor Georgiev and Andrew Lumsdaine. Focused plenoptic camera and rendering. *Journal of Electronic Imaging*, 19(2):021106–021106, 2010.

[4] Levoy Mark. Stanford light field microscope project, 2005.

[5] Joseph Carroll, David B Kay, Drew Scoles, Alfredo Dubra, and Marco Lombardo. Adaptive optics retinal imaging-clinical opportunities and challenges. *Current eye research*, 38(7):709–721, 2013.

[6] Gordon Wetzstein, Ivo Ihrke, Douglas Lanman, and Wolfgang Heidrich. Computational plenoptic imaging. In *Computer Graphics Forum*, volume 30, pages 2397–2426. Wiley Online Library, 2011.

[7] Edward H Adelson and James R Bergen. *The plenoptic function and the elements of early vision*. Vision and Modeling Group, Media Laboratory, Massachusetts Institute of Technology, 1991.

[8] Edward H Adelson and John Y. A. Wang. Single lens stereo with a plenoptic camera. *IEEE Transactions on Pattern Analysis & Machine Intelligence*, (2):99–106, 1992.

[9] Plato and Francis Macdonald Cornford. *The republic of Plato*, volume 30. Oxford University Press New York, 1945.

[10] Herbert E Ives. Parallax panoramagrams made with a large diameter lens. *J. Opt. Soc. Amer*, 20:332–342, 1930.

[11] Frederic E Ives. Parallax stereogram and process of making same., April 14 1903. US Patent 725,567.

[12] Lippmann Gabriel. La photographie intégrale. *Comptes-Rendus, Académie des Sciences*, 146:446–551, 1908.

[13] Marc Levoy and Pat Hanrahan. Light field rendering. In *Proceedings of the 23rd annual conference on Computer graphics and interactive techniques*, pages 31–42. ACM, 1996.

[14] Yuichi Taguchi, Amit Agrawal, Srikumar Ramalingam, and Ashok Veeraraghavan. Axial light field for curved mirrors: Reflect your perspective, widen your view. In *Computer Vision and Pattern Recognition (CVPR), 2010 IEEE Conference on*, pages 499–506. IEEE, 2010.

[15] Steven J Gortler, Radek Grzeszczuk, Richard Szeliski, and Michael F Cohen. The lumigraph. In *Proceedings of the 23rd annual conference on Computer graphics and interactive techniques*, pages 43–54. ACM, 1996.

[16] Bennett S Wilburn, Michal Smulski, Hsiao-Heng K Lee, and Mark A Horowitz. Light field video camera. In *Electronic Imaging 2002*, pages 29–36. International Society for Optics and Photonics, 2001.

[17] Jason C Yang, Matthew Everett, Chris Buehler, and Leonard McMillan. A real-time distributed light field camera. *Rendering Techniques*, 2002:77–86, 2002.

[18] Yoshikuni Nomura, Li Zhang, and Shree K Nayar. Scene collages and flexible camera arrays. In *Proceedings of the 18th Eurographics conference on Rendering Techniques*, pages 127–138. Eurographics Association, 2007.

[19] Todor Georgiev, Ke Colin Zheng, Brian Curless, David Salesin, Shree Nayar, and Chintan Intwala. Spatio-angular resolution tradeoffs in integral photography. *Rendering Techniques*, 2006:263–272, 2006.

[20] Massimo Turola and Steve Gruppetta. Wave optics simulations of a focused plenoptic system. In *Frontiers in Optics*, pages JTu3A–24. Optical Society of America, 2014.

[21] Ren Ng, Marc Levoy, Mathieu Brédif, Gene Duval, Mark Horowitz, and Pat Hanrahan. Light field photography with a hand-held plenoptic camera. *Computer Science Technical Report CSTR*, 2(11), 2005.

[22] Kensuke Ueda, Takafumi Koike, Keita Takahashi, and Takeshi Naemura. Adaptive integral photography imaging with variable-focus lens array. In *Electronic Imaging 2008*, pages 68031A–68031A. International Society for Optics and Photonics, 2008.

[23] Ashok Veeraraghavan, Ramesh Raskar, Amit Agrawal, Ankit Mohan, and Jack Tumblin. Dappled photography: Mask enhanced cameras for heterodyned light fields and coded aperture refocusing. *ACM Trans. Graph.*, 26(3):69, 2007.

[24] Douglas Lanman, Ramesh Raskar, Amit Agrawal, and Gabriel Taubin. Shield fields: modeling and capturing 3d occluders. *ACM Transactions on Graphics (TOG)*, 27(5):131, 2008.

[25] Kshitij Marwah, Gordon Wetzstein, Yosuke Bando, and Ramesh Raskar. Compressive light field photography using overcomplete dictionaries and optimized projections. *ACM Transactions on Graphics (TOG)*, 32(4):46, 2013.

[26] Yu Ji, Jinwei Ye, and Jingyi Yu. Depth reconstruction from the defocus effect of an xslit camera. In *Computational Optical Sensing and Imaging*, pages CM4E–3. Optical Society of America, 2015.

[27] Todor Georgiev and Andrew Lumsdaine. The multifocus plenoptic camera. In *IS&T/SPIE Electronic Imaging*, pages 829908–829908. International Society for Optics and Photonics, 2012.

[28] Todor Georgiev and Chintan Intwala. Light field camera design for integral view photography. *Adobe System, Inc*, 2006.

[29] Tom E Bishop, Sara Zanetti, and Paolo Favaro. Light field superresolution. In *Computational Photography (ICCP), 2009 IEEE International Conference on*, pages 1–9. IEEE, 2009.

[30] Sapna A Shroff and Kathrin Berkner. Image formation analysis and high resolution image reconstruction for plenoptic imaging systems. *Applied optics*, 52(10):D22–D31, 2013.

[31] Todor Georgiev and Andrew Lumsdaine. Superresolution with plenoptic camera 2.0. *Adobe Systems Incorporated, Tech. Rep*, 2009.

[32] Todor Georgiev. Plenoptic camera resolution. In *Computational Optical Sensing and Imaging*, pages JTh4A–2. Optical Society of America, 2015.

[33] Changyin Zhou and Shree K Nayar. Computational cameras: Convergence of optics and processing. *Image Processing, IEEE Transactions on*, 20(12):3322–3340, 2011.

[34] Andrew Lumsdaine and Todor Georgiev. Full resolution lightfield rendering. *Indiana University and Adobe Systems, Tech. Rep*, 2008.

[35] Andrew Lumsdaine and Todor Georgiev. The focused plenoptic camera. In *Computational Photography (ICCP), 2009 IEEE International Conference on*, pages 1–8. IEEE, 2009.

[36] Tom E Bishop and Paolo Favaro. Full-resolution depth map estimation from an aliased plenoptic light field. In *Computer Vision–ACCV 2010*, pages 186–200. Springer, 2011.

[37] Todor G Georgiev and Andrew Lumsdaine. Resolution in plenoptic cameras. In *Computational Optical Sensing and Imaging*, page CTuB3. Optical Society of America, 2009.

[38] Victor Guillemin and Shlomo Sternberg. *Symplectic techniques in physics*. Cambridge University Press, 1990.

[39] Todor Georgiev, Andrew Lumsdaine, and Sergio Goma. Plenoptic principal planes. In *Imaging Systems and Applications*, page JTuD3. Optical Society of America, 2011.

[40] Sapna Shroff and Kathrin Berkner. High resolution image reconstruction for plenoptic imaging systems using system response. In *Computational Optical Sensing and Imaging*, pages CM2B–2. Optical Society of America, 2012.

[41] Gabriel C Birch, J Scott Tyo, and Jim Schwiegerling. Depth measurements through controlled aberrations of projected patterns. *Optics express*, 20(6):6561–6574, 2012.

[42] Joyce E Farrell, Peter B Catrysse, and Brian A Wandell. Digital camera simulation. *Applied Optics*, 51(4):A80–A90, 2012.

[43] Brian S Thurow and Timothy Fahringer. Recent development of volumetric piv with a plenoptic camera. In *PIV13; 10th International Symposium on Particle Image Velocimetry, Delft, The Netherlands, July 1-3, 2013*. Delft University of Technology, Faculty of Mechanical, Maritime and Materials Engineering, and Faculty of Aerospace Engineering, 2013.

[44] Kyle Lynch. *Development of a 3-D fluid velocimetry technique based on light field imaging*. PhD thesis, Auburn University, 2011.

[45] Kyle Lynch, Tim Fahringer, and Brian Thurow. Three-dimensional particle image velocimetry using a plenoptic camera. In *AIAA Aerospace Sciences Meeting*, 2012.

[46] Arnold Sommerfeld. Optics lectures on theortical physics, vol. iv. *Optics Lectures on Theortical Physics, Vol. IV by Arnold Sommerfeld New York, NY: Academic Press INC, 1954*, 1, 1954.

[47] Joseph W Goodman. *Introduction to Fourier optics*. Roberts and Company Publishers, 2005.

[48] Maciej Sypek. Light propagation in the fresnel region. new numerical approach. *Optics communications*, 116(1):43–48, 1995.

[49] Rafael C Gonzalez, Richard Eugene Woods, and Steven L Eddins. *Digital image processing using MATLAB*. Pearson Education India, 2004.

[50] Kyoji Matsushima and Tomoyoshi Shimobaba. Band-limited angular spectrum method for numerical simulation of free-space propagation in far and near fields. *Optics express*, 17(22):19662–19673, 2009.

[51] Maciej Sypek. Reply to the comment on "light propagation in the fresnel region–new numerical approach". *Optics Communications*, 282(6):1074–1077, 2009.

[52] Frank L Pedrotti and Leno S Pedrotti. Introduction to optics 2nd edition. *Introduction to Optics 2nd Edition by Frank L. Pedrotti, SJ, Leno S. Pedrotti New Jersey: Prentice Hall, 1993*, 1, 1993.

[53] Joseph W Goodman and Randy L Haupt. *Statistical optics*. John Wiley & Sons, 2015.

[54] Leonard Mandel and Emil Wolf. *Optical coherence and quantum optics*. Cambridge university press, 1995.

[55] Max Born and Emil Wolf. *Principles of optics: electromagnetic theory of propagation, interference and diffraction of light*. Cambridge university press, 1999.

[56] Emil Wolf. *Introduction to the Theory of Coherence and Polarization of Light*. Cambridge University Press, 2007.

[57] Kensuke Ueda, Dongha Lee, Takafumi Koike, Keita Takahashi, and Takeshi Naemura. Multi-focal compound eye: liquid lens array for computational photography. In *ACM SIGGRAPH 2008 new tech demos*, page 28. ACM, 2008.

[58] Todor G Georgiev and Andrew Lumsdaine. Super-resolution with the focused plenoptic camera, November 20 2012. US Patent 8,315,476.

[59] Christian Perwass and Lennart Wietzke. Single lens 3d-camera with extended depth-of-field. In *Proc. SPIE*, volume 8291, page 829108, 2012.

[60] Michael Hansen and Eric Holk. Depth map estimation for plenoptic images. 2011.

[61] Ole Johannsen, Christian Heinze, Bastian Goldluecke, and Christian Perwaß. On the calibration of focused plenoptic cameras. In *Time-of-*

Flight and Depth Imaging. Sensors, Algorithms, and Applications, pages 302–317. Springer, 2013.

[62] Hans Peter Herzig. *Micro-optics: elements, systems and applications*. CRC Press, 1997.

[63] Todor Georgiev, Georgi Chunev, and Andrew Lumsdaine. Superresolution with the focused plenoptic camera. In *IS&T/SPIE Electronic Imaging*, pages 78730X–78730X. International Society for Optics and Photonics, 2011.

[64] Todor G Georgiev, Andrew Lumsdaine, and Sergio Goma. High dynamic range image capture with plenoptic 2.0 camera. In *Signal recovery and synthesis*, page SWA7P. Optical Society of America, 2009.

[65] Paolo Favaro. A split-sensor light field camera for extended depth of field and superresolution. In *SPIE Photonics Europe*, pages 843602–843602. International Society for Optics and Photonics, 2012.

[66] Tom E Bishop and Paolo Favaro. The light field camera: Extended depth of field, aliasing, and superresolution. *Pattern Analysis and Machine Intelligence, IEEE Transactions on*, 34(5):972–986, 2012.

[67] Chien-Hung Lu, Stefan Muenzel, and Jason Fleischer. High-resolution light-field microscopy. In *Computational Optical Sensing and Imaging*, pages CTh3B–2. Optical Society of America, 2013.

[68] Vivek Boominathan, Kaushik Mitra, and Ashok Veeraraghavan. Improving resolution and depth-of-field of light field cameras using a hybrid

imaging system. In *Computational Photography (ICCP), 2014 IEEE International Conference on*, pages 1–10. IEEE, 2014.

[69] Photonics for Iinnovations Quioptiq. *The Linos Catalog*. 2015.

[70] August Köhler. A new system of illumination for photomicrographic purposes. *Z. Wiss. Mikroskopie*, 10:433–440, 1893.

[71] August Kohler and Walter Bauersfeld. Device for light-field and dark-field illumination of microscopic objects, January 16 1934. US Patent 1,943,510.

[72] Kurt Bernardo Wolf. *Geometric optics on phase space*. Springer Science & Business Media, 2004.